Supplement of Atmos. Chem. Phys., 26, 8695–8715, 2026
https://doi.org/10.5194/acp-26-8695-2026-supplement

Atmospheric Chemistry and Physics
Open Access
EGU

Supplement of

Wintertime photochemistry of acyl peroxynitrates and ozone in South Korea during the ASIA-AQ campaign

Young Ro Lee et al.

Correspondence to: L. Gregory Huey (greg.huey@eas.gatech.edu)

S1 Airborne observations during the ASIA-AQ campaign and data processing

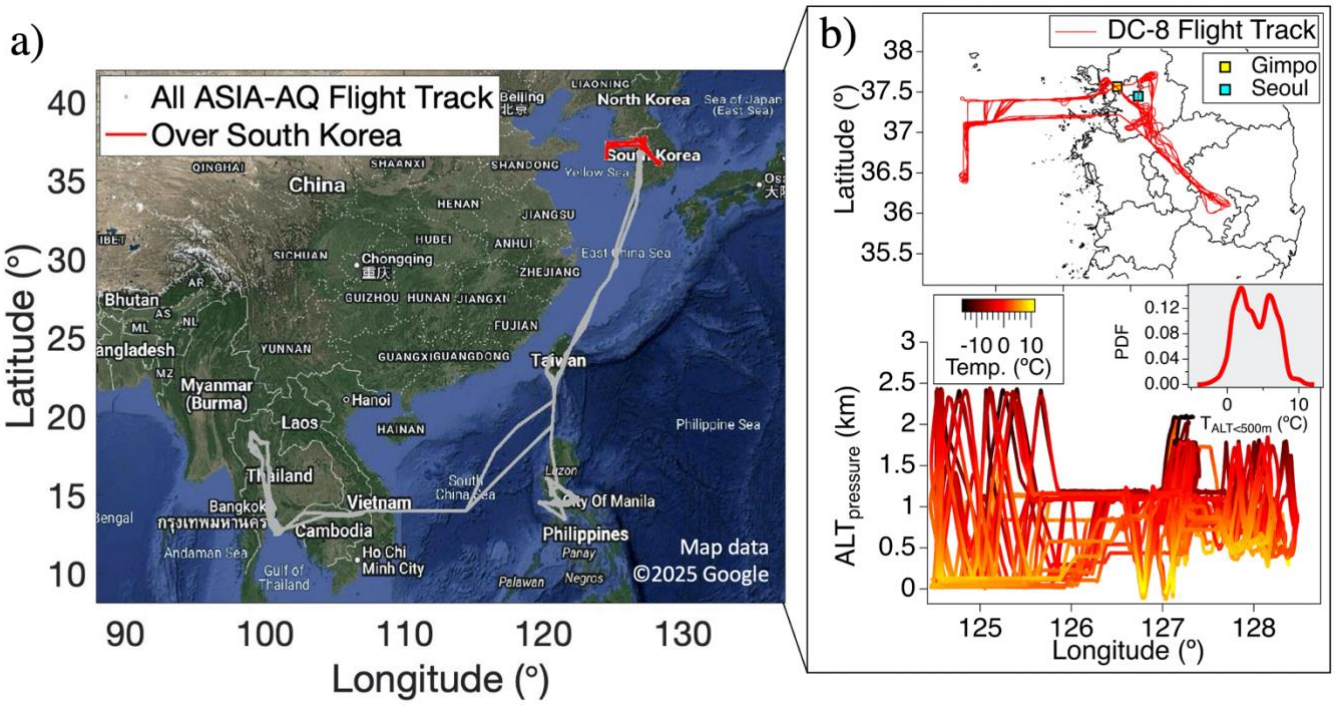

Figure S1. (a) Map of DC-8 flight paths for ASIA-AQ shown in grey, with the South Korea flights in red. (b) (top) The red line shows the DC-8 flight paths over South Korea, with yellow and cyan squares indicating Gimpo and Seoul Airports, respectively, which were used for low approaches. (bottom) Plot of altitude as a function of longitude and colored by temperature. The inset illustrates the probability distribution function (PDF) of temperature measured at altitudes below 500 m.

Table S1. Aircraft measurements aboard the NASA DC-8 aircraft used in this study.

Measurement	Instrument	Uncertainty	Reference
Acyl peroxynitrates (PANs)	Georgia Tech Thermal Dissociation Chemical Ionization Mass Spectrometry (GT TD-CIMS) using I^- reagent ion	10–30%	Slusher et al. (2004); Ji et al. (2020) Lee et al. (2019)
NO	Chemiluminescence	8%	Weinheimer et al. (1994)
NO_2	Compact Airborne NO_2 Experiment (CANOE)	10% ± 120 pptv	St. Clair et al. (2019); Bourgeois et al. (2022)
O_3	Rapid OZone Experiment (ROZE)	6.2%	Hannun et al. (2020)
CO, CH_4	Differential Absorption Carbon monOxide Measurement (DACOM)	2–5%, 1%	Sachse et al. (1987, 1991)
Relative humidity	Diode Laser Hygrometer measurements of H_2O	15%	Diskin et al. (2002)
Ethane, alkenes, ethyltoluenes, trimethylbenzenes, α-pinene, β-pinene	Whole Air Sampling and Gas Chromatography (WAS and GC)	5%	Simpson et al. (2020)
C_8-romatics, benzaldehyde	Proton-transfer reaction mass spectrometer	15%	Reinecke et al. (2023)
Volatile organic compounds (VOCs), oxygenated VOCs, isopropyl nitrate	NSF NCAR Trace Organic Mass Analyzer with time-of-flight mass spectrometer (TOGA-TOF)	15–40%	Apel et al. (2015); Hornbrook et al. (2016)
Formaldehyde (CH_2O)	In Situ Airborne Formaldehyde (ISAF)	10% + 10 pptv	Cazorla et al. (2015)
Particle concentrations (volume, number density, surface area)[a]	Ultra-High Sensitivity Aerosol Spectrometer (Droplet Measurement Technology UHSAS), Aerodynamic Particle Sizer (APS; TSI 3321), and Scanning Mobility Particle Sizer (SMPS; TSI model 3776)	20%	Moore et al. (2021)
HNO_3, HCN, phenol, cresol, nitrophenol, nitrocresol	Caltech Chemical Ionization Mass Spectrometer (CIT-CIMS) using CF_3O^- reagent ion	20% ± 25 pptv, 25% ± 35 pptv, 30% ± 20 pptv, 30% ± 10 pptv, 30% ± 10 pptv, 30% ± 10 pptv	Crounse et al. (2006)
Organic aerosol (OA), particulate nitrate (pNO_3^-)	Aerosol Mass Spectrometer	19%, 18%	Bahreini et al. (2009); Nault et al. (2018); Guo et al. (2021)
Photolysis frequencies (*j* values)	Charged-coupled device Actinic Flux Spectroradiometers (CAFS)	12% *j*-NO_2, 20% *j*-O_3, *j*(Acetone, MEK, BIACET)-20%, 20%, 16%	Hall et al. (2018)

[a]Aerosol measurements target different aerosol size range where APS, UHSAS and SMPS targets approximately 0.5–5 μm, 60–1000 nm and 3–80 nm.

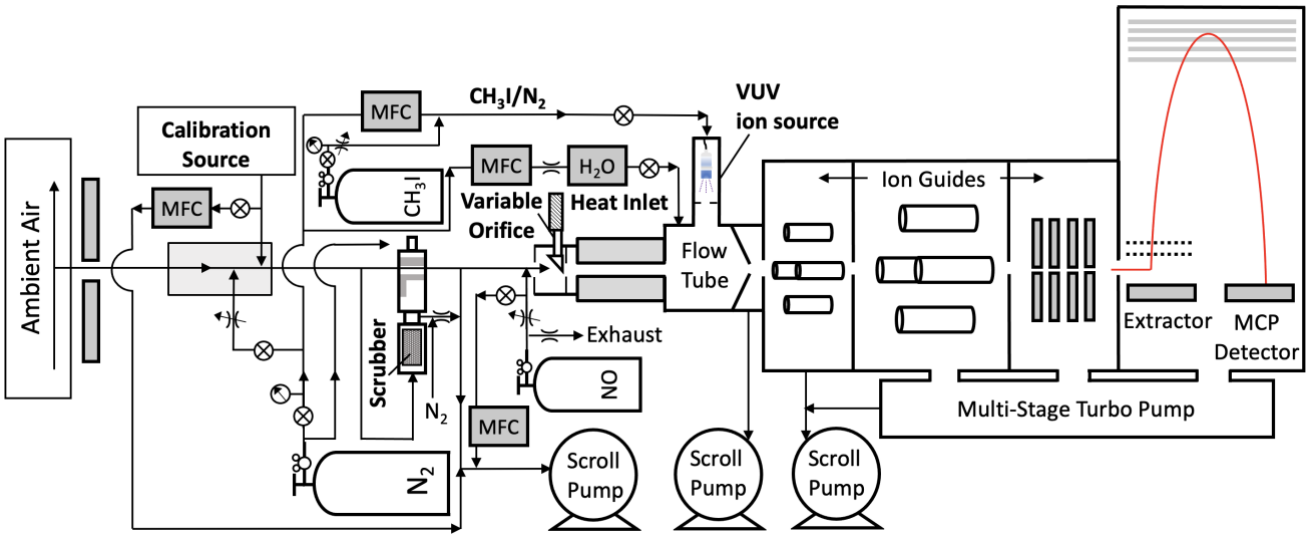

Figure S2. Schematic diagram of the Thermal Dissociation-Chemical Ionization Mass Spectrometer (TD-CIMS).

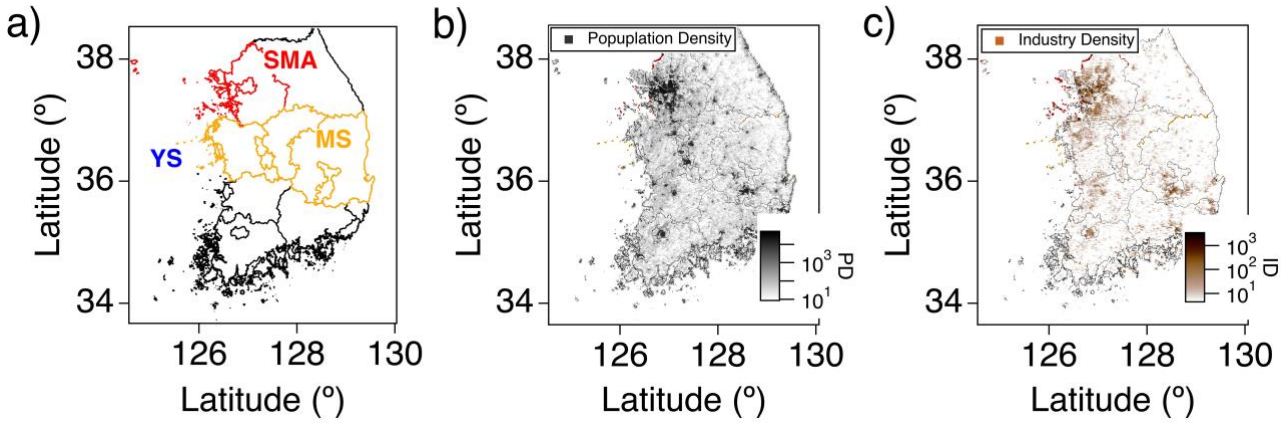

Figure S3. (a) Map of South Korea with geographic boundaries used to filter data. The Seoul Metropolitan Area (SMA) includes Seoul and suburban regions (Incheon and Gyeonggi provinces). The Mid and South (MS) region includes northern and southern Chungcheong provinces, Sejong, and northern Gyeongsang province. The Yellow Sea (YS) is the region to the west of the Korean Peninsula. (b) Map of South Korea colored by 1 km^2 population density (PD). (c) Map of South Korea colored by 1 km^2 industrial facility density (ID).

S2 Kinetic calculations for instantaneous production rates

Table S2. Volatile organic compounds (VOCs) used in kinetic calculations with corresponding hydroxyl radical (OH) reaction rate coefficients (k_{OH}), ozone yields (ϒ) and alkyl nitrate branching ratios (α). For acetaldehyde, acrolein and i-butanal, α denotes hydrogen abstraction ratios.

	k_{OH} @ 298 K[a]	ϒ[b]	α[c]		k_{OH} @ 298 K	ϒ[b]	α[c]
Alkanes							
Ethane	2.48×10^{-13}	2.00	0.019	2-Methylpentane	5.3×10^{-12}	2.85	0.097
Propane	1.09×10^{-12}	2.00	0.036	3-Methylpentane	5.4×10^{-12}	2.85	0.109
n-Butane	2.36×10^{-12}	2.85	0.077	n-Heptane	6.76×10^{-12}	2.85	0.178
i-Butane	2.12×10^{-12}	2.85	0.096	n-Octane	8.11×10^{-12}	2.85	0.226
n-Pentane	3.8×10^{-12}	2.85	0.105	n-Nonane	9.7×10^{-12}	2.85	0.393
i-Pentane	3.6×10^{-12}	2.85	0.07	2,2,4-Trimethylpentane	3.34×10^{-12}	2.85	0.14
n-Hexane	5.2×10^{-12}	2.85	0.141				
Alkenes				**Aromatics**			
Ethene	8.52×10^{-12}	2	0.013[d]	Benzene	1.22×10^{-12}	2	0.034
Propene	2.63×10^{-11}	2	0.041[d]	Toluene	5.63×10^{-12}	2	0.029
1-Butene	3.14×10^{-11}	2	0.12[d]	Ethylbenzene	7×10^{-12}	2	0.072
cis-2-Butene	5.64×10^{-11}	2	0.12[d]	(m + p)-Xylenes	1.87×10^{-11}	2	0.086
trans-2-Butene	6.4×10^{-11}	2	0.12[d]	o-Xylene	1.36×10^{-11}	2	0.081
1,3-Butadiene	6.66×10^{-11}	2	0.10[d]	Styrene	5.8×10^{-11}	2	0.1
1-Pentene	3.14×10^{-11}	2	0.15[d]	1,2,3-Trimethylbenzene	3.3×10^{-11}	2	0.105
α-Pinene	5.25×10^{-11}	2.85	0.18	1,2,4-Trimethylbenzene	3.3×10^{-11}	2	0.119
β-Pinene	7.89×10^{-11}	2.85	0.24	1,3,5-Trimethylbenzene	5.7×10^{-11}	2	0.031
				2-Ethyltoluene	1.19×10^{-11}	2	0.106
				3-Ethyltoluene	1.86×10^{-11}	2	0.094
				4-Ethyltoluene	1.18×10^{-11}	2	0.137
Oxygenated Species							
CO	2.39×10^{-13}	1	-	Benzaldehyde	1.26×10^{-11}	2.85	-
Formaldehyde	8.37×10^{-12}	1	-	Methyl formate	2×10^{-13}	2	-
Formaldehyde (hv)	-	2	-	Methyl acetate	3.49×10^{-13}	2	-
Acetaldehyde	1.58×10^{-11}	3	0.95[e]	Ethyl acetate	1.68×10^{-12}	2	-
Acrolein	2×10^{-11}	2.85	0.68[e]	Acetone	1.75×10^{-13}	2.85	-
Propanal	1.91×10^{-11}	2.85	-	MEK	1.11×10^{-12}	2	-
Butanal	2.38×10^{-11}	2.85	-	Methanol	9×10^{-13}	1	-
i-Butanal	2.69×10^{-11}	2.85	0.887[e]	Ethanol	3.21×10^{-12}	1	-
Pentanal	2.85×10^{-11}	2.85	-	i-Propanol	5.09×10^{-12}	1	-
Butenal	3.4×10^{-11}	2.85	-	MVK	2.01×10^{-11}	2	0.11
Methacrolein	2.86×10^{-11}	2.5	0.15	BIACET	2.39×10^{-13}	2	-
Other							
CH_4	6.34×10^{-15}	2	-	Ethyne	8.74×10^{-13}	1.2	0.09

[a]Reaction rate coefficients with OH (k_{OH}, in units of cm^3 $molecule^{-1}$ s^{-1}) from the Master Chemical Mechanism (MCM) v3.3.1, consistent with IUPAC recommendation.
[b]Ozone yields from Rosen et al. (2004).

[c]Alkyl nitrate branching ratios adapted from Perring et al. (2013) unless noted otherwise.
[d]Hydroxynitrates branching ratios from Teng et al. (2015).
[e]Hydrogen abstraction branching ratios for the selected aldehydes.

S3 Observational constraints for 0-D box model simulations and sensitivity analysis

Table S3. Airborne observations used to constrain flight steady-state box model simulations and corresponding compound name in MCM v3.3.1.

Observations	Instrument	MCM name	Observation	Instrument	MCM name
non-VOCs					
O_3	ROZE	O3	PPN	GT TD-CIMS	PPN
NO	Chemiluminescence	NO	PBN	GT TD-CIMS	PIPN
NO_2	CANOE	NO2	APAN	GT TD-CIMS	ACRPAN
H_2O_2	CIT-CIMS	H2O2	PBzN	GT TD-CIMS	PBZN
PAN	GT TD-CIMS	PAN			
VOCs					
CO	DACOM	CO	1,2,3-Trimethylbenzene	WAS	TM123B
Ethyne	WAS	C2H2	1,2,4-Trimethylbenzene	WAS	TM124B
Ethene	WAS	C2H4	1,3,5-Trimethylbenzene	WAS	TM135B
Propene	WAS	C3H6	CH_4	DACOM	CH4
1-Butene	WAS	BUT1ENE	CH_2O	ISAF	HCHO
i-Butene	WAS	MEPROPENE	Methyl formate	TOGA	CH3OCHO
cis-2-Butene	WAS	CBUT2ENE	Methyl acetate	TOGA	METHACET
trans-2-Butene	WAS	TBUT2ENE	Ethyl acetate	TOGA	ETHACET
1,3-Butadiene	WAS	C4H6	Acetone	TOGA	CH3COCH3
1-Pentene	WAS	C5H8	MEK	TOGA	MEK
Ethane	WAS	C2H6	Methanol	TOGA	CH3OH
Propane	TOGA	C3H8	Ethanol	TOGA	C2H5OH
n-Butane	TOGA	NC4H10	i-Propanol	TOGA	IPROPOL
i-Butane	TOGA	IC4H10	MVK	TOGA	MVK
i-Pentane	TOGA	IC5H12	2,3-Butanedione	TOGA	BIACET
n-Pentane	TOGA	NC5H12	2-Pentanone	TOGA	MPRK
n-Hexane	TOGA	NC6H14	3-Pentanone	TOGA	DIEK
n-Heptane	TOGA	NC7H16	Acetaldehyde	TOGA	CH3CHO
n-Octane	TOGA	NC8H18	Propanal	TOGA	C2H5CHO
n-Nonane	TOGA	NC9H20	Butanal	TOGA	C3H7CHO
Benzene	TOGA	BENZENE	i-Butanal	TOGA	IPRCHO
Toluene	TOGA	TOLUENE	Acrolein	TOGA	ACR
Ethylbenzene	TOGA	EBENZ	Benzaldehyde	PTR-MS	BENZAL
o-Xylene	TOGA	OXYL	Pentanal	TOGA	C4H9CHO
m-Xylene	TOGA	MXYL	Methacrolein	TOGA	MACR
p-Xylene	TOGA	PXYL	2-Butenals	TOGA	C4ALD8
2-Ethyltoluene	WAS	OETHTOL	α-Pinene	WAS	APINENE
3-Ethyltoluene	WAS	METHTOL	β-Pinene	WAS	BPINENE
4-Ethyltoluene	WAS	PETHTOL	Styrene	TOGA	STYRENE

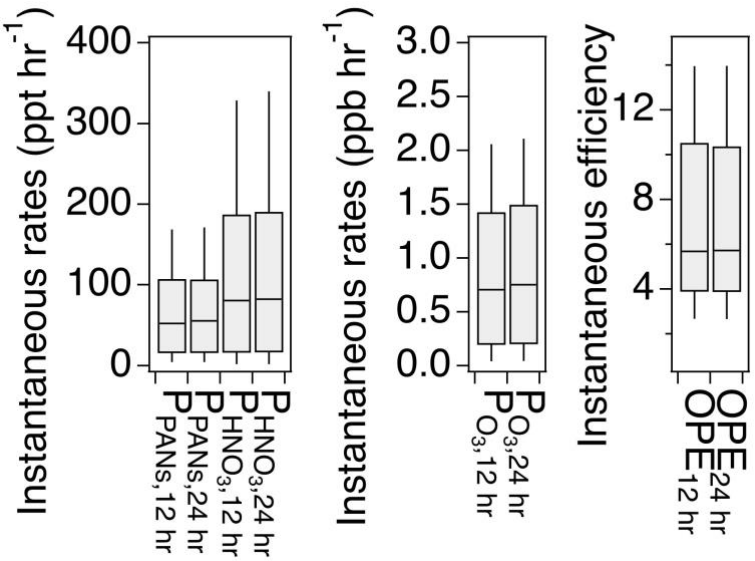

Figure S4. Box plots for modeled *P*(PANs), *P*(HNO_3), *P*(O_3) and OPE using 12-hour and 24-hour lifetimes.

35

S4 Correlations of PANs with gaseous and particulate compounds over the campaign domain

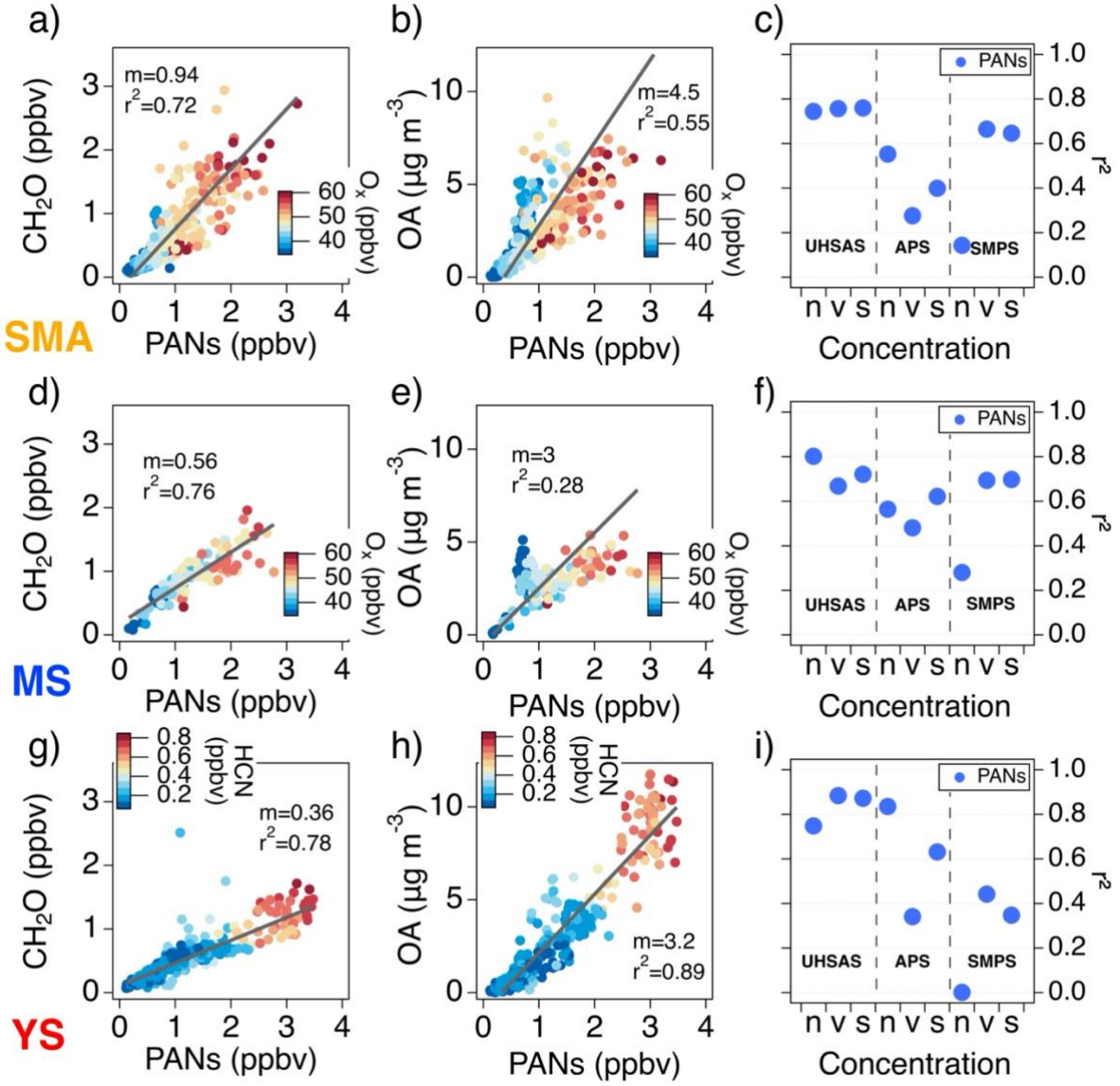

Figure S5. Scatter plots of PANs with (a, d, g) CH_2O and (b, e, h) OA over the SMA, MS and YS, respectively, along with linear regression slopes (m) and r^2 values. Markers are colored by odd oxygen (O_x; defined as $O_3 + NO_2$) for the SMA and MS and by HCN for the YS. Right panels (c, f, i) show r^2 values for correlations between PANs and aerosol number (n), volume (v), and surface area (s) concentrations measured by the Ultra-High Sensitivity Aerosol Spectrometer (UHSAS), Aerodynamic Particle Sizer (APS), and Scanning Mobility Particle Sizer (SMPS) over the SMA, MS and YS, respectively.

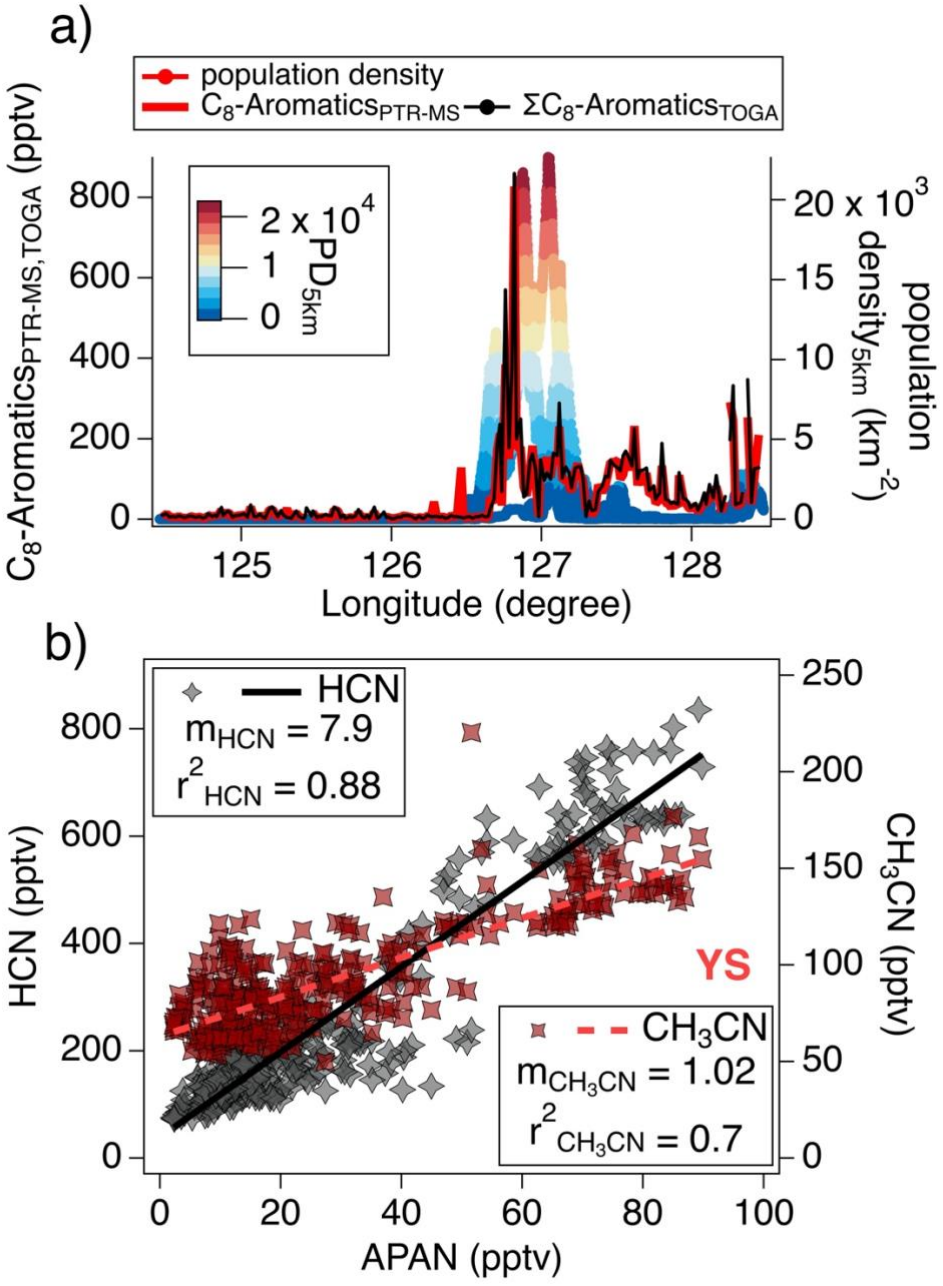

Figure S6. (a) Longitudinal distribution of median C_8-aromatics measured by PTR-MS and TOGA-TOF in 0.02º longitude bins (left axis), along with population density within 5-km of the DC-8 measurements (PD_{5km}) (right axis). (b) Scatter plots of HCN and CH_3CN versus APAN observed over YS, shown on the left and right axes, respectively.

S5 Additional kinetic calculations

S5.1 Estimation of OH exposure

To incorporate a qualitative measure of the degree of photochemical processing in air masses, we estimate OH exposure (OHΔt), defined as the product of OH concentration and time, averaged over the photochemical age of an air mass (McKeen and Liu, 1993; Parrish et al., 2007). This estimation is based on the ratio of alkanes to their corresponding alkyl nitrates (ANs) in parent-daughter relationships, using Eq. (S1) (Bertman et al., 1995; Farmer et al., 2011; Romer et al., 2018). With the assumption that the ANs are produced exclusively from secondary formation of parent oxidation, the term for initial conditions in Eq. (S1) can be neglected (Bertman et al., 1995). This approach is particularly advantageous over an alternative method that estimate OHΔt from the relative decay of VOC pairs with distinct atmospheric lifetimes, as the alternative method requires initial conditions (i.e., emission ratios), which are difficult to constrain in regions with complex source characteristics such as South Korea.

Specifically, we use the observed ratio of isopropyl nitrate (IPN) to propane for the OHΔt estimation. IPN is the dominant form of propyl nitrate, almost exclusively formed from oxidation of propane (Fischer et al., 2018). With increasing degree of photochemical processing, the isopropyl nitrate to propane ratio is expected to increase. In Eq. (S1), the alkyl nitrate branching ratios of propane (α_{propane}) are from Perring et al. (2013) (Table S2), and χ_{H-abs} represents the fraction of hydrogen abstraction (0.736) by OH from the secondary carbon of propane, adapted from MCM v.3.3.1, leading to isopropyl peroxy radical.

$$[\text{OH}]\Delta t = \frac{1}{k_{\text{Propane+OH}} - k_{\text{IPN+OH}}} \ln\left(1 - \frac{\text{IPN}}{\text{Propane}}\left(\frac{k_{\text{IPN+OH}} - k_{\text{Propane+OH}}}{\chi_{H-abs}\alpha_{propane}k_{\text{Propane+OH}}}\right)\right) \quad \text{(S1)}$$

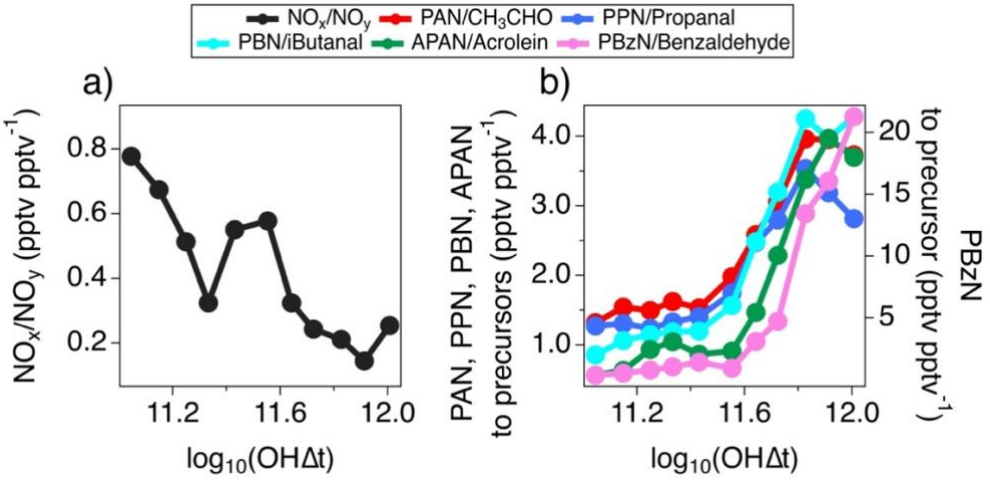

Figure S7. (a) The median ratios of NO_x to NO_y (approximated as PANs + HNO_3 + pNO_3^-) as a function of logarithmic OH exposure. (b) The median ratios of PANs to corresponding aldehyde precursor as a function of logarithmic OH exposure.

S5.2 Inferred *P*(PAN) from non-acetaldehyde sources

Production rates of PAN (*P*(PAN)) from non-acetaldehyde precursors (inferred $P(\mathrm{PAN})_{\mathrm{w/o\ CH3CHO}}$) were estimated using kinetic calculations in Eq. (S2) and Eq. (S3). This approach assumes that the observed PAN-to-homologue ratios reflect the relative rates of their local production at the point of measurement. In Eq. (S2), the observed PAN-to-homologue ratios are equated to the relative production rates of PAN to PAN homologues, with *P*(PAN) expressed as the sum of production rates from oxidation of acetaldehyde and non-acetaldehyde precursors, $P(\mathrm{PAN})_{\mathrm{CH3CHO}}$ and $P(\mathrm{PAN})_{\mathrm{w/o\ CH3CHO}}$, respectively. Rearranging Eq. (S2) for $P(\mathrm{PAN})_{\mathrm{w/o\ CH3CHO}}$ yields Eq. (S3), in which $P(\mathrm{PAN})_{\mathrm{w/o\ CH3CHO}}$ is expressed as the product of the observed PAN-to-homologue ratio and the production rates of homologues, subtracted by $P(\mathrm{PAN})_{\mathrm{CH3CHO}}$. The inferred $P(\mathrm{PAN})_{\mathrm{w/o\ CH3CHO}}$ from Eq. (S3) is used to provide an independent observational constraint on precursor contributions to *P*(PAN), complementing model-based estimates.

$$\frac{\mathrm{PAN}}{\mathrm{PAN\ homologues}} = \frac{\beta_{\mathrm{PAN}}\ (k_{OH+CH3CHO}[\mathrm{OH}][\mathrm{CH3CHO}]) + P(PAN)_{\mathrm{w/o\ CH3CHO}}}{\beta_{\mathrm{PAN}}\ \alpha_{\mathrm{H\ abs,\ PAN\ homologues}} k_{\mathrm{OH+OVOC_{PAN\ homologues}}}[\mathrm{OH}][\mathrm{OVOC}]_{\mathrm{PAN\ homologues}}}$$

$$\text{, where } \beta_{\mathrm{PAN}} = \frac{k_{\mathrm{PA+NO_2}}[\mathrm{NO_2}]}{k_{\mathrm{PA+NO_2}}[\mathrm{NO_2}] + k_{\mathrm{PA+NO}}[\mathrm{NO}]} \tag{S2}$$

$$P(\mathrm{PAN})_{\mathrm{w/o\ CH3CHO}} = \frac{\mathrm{PAN}(\beta_{\mathrm{PAN}}\alpha_{\mathrm{Hydrogen\ abstraction,\ PAN\ homologues}} k_{\mathrm{OH+OVOC_{PAN\ homologues}}}[\mathrm{OH}][\mathrm{OVOC}]_{\mathrm{PAN\ homologues}})}{\mathrm{PAN\ homologues}} - \beta_{PAN}\ (k_{\mathrm{OH+CH3CHO}}[\mathrm{OH}][\mathrm{CH3CHO}]) \tag{S3}$$

S5.3 Kinetic investigation on relative NO_x loss pathways

We investigate the fractional contribution of PANs production to total NO_x loss ($\chi_{\mathrm{PANs-kc}}$) using the kinetic calculations described in Eq. (S4)–Eq. (S6). $\chi_{\mathrm{PANs-kc}}$ is defined as the production rate of PANs relative to the sum of PANs (P(PANs)) and HNO_3 ($P(HNO_3)$) production rates, with both terms derived from Eq. (4) and Eq. (5) in the main manuscript. Following Eq. (1), the OH reactivity of NO_2 and aldehydes can be expressed as R_{NO2} and R_{ALD}, respectively, allowing Eq. (S4) to be simplified to Eq. (S5). Substituting the explicit form of β_{PANs}, shown in Eq. (S2), and normalizing by R_{ALD} yields Eq. (S6). This equation predicts a negative dependence of $\chi_{\mathrm{PANs-kc}}$ on both R_{NO2}/R_{ALD} and NO/R_{ALD} broadly reflecting the ratio of NO_x to aldehydes. The contribution of the OVOC photolysis term (J_{OVOCs}[OVOCs]) to $\chi_{\mathrm{PANs-kc}}$ is minimal (<2% increase in $\chi_{\mathrm{PANs-kc}}$ for a factor of two increase in J_{OVOCs}[OVOCs]), because it is divided by much larger values (i.e., R_{ALD}[OH]) and appears in both numerator and denominator.

$$\frac{P(\mathrm{PANs})}{P(\mathrm{HNO_3})+P(\mathrm{PANs})}=\frac{\beta_{\mathrm{PANs}}(k_{\mathrm{OH+Aldehydes}}[\mathrm{Aldehydes}][\mathrm{OH}]+J_{\mathrm{OVOCs}}[\mathrm{OVOCs}])}{k_{\mathrm{OH+NO_2}}[\mathrm{NO_2}][\mathrm{OH}]+\beta_{\mathrm{PANs}}(k_{\mathrm{OH+Aldehydes}}[\mathrm{Aldehydes}][\mathrm{OH}]+J_{\mathrm{OVOCs}}[\mathrm{OVOCs}])} \quad \text{(S4)}$$

$$\frac{P(\mathrm{PANs})}{P(\mathrm{HNO_3})+P(\mathrm{PANs})}=\frac{\beta_{\mathrm{PANs}}R_{\mathrm{ALD}}[\mathrm{OH}]+J_{\mathrm{OVOCs}}[\mathrm{OVOCs}])}{R_{\mathrm{NO_2}}[\mathrm{OH}]+\beta_{\mathrm{PANs}}R_{\mathrm{ALD}}[\mathrm{OH}]+J_{\mathrm{OVOCs}}[\mathrm{OVOCs}])} \quad \text{(S5)}$$

$$\frac{P(\mathrm{PANs})}{P(\mathrm{HNO_3})+P(\mathrm{PANs})}=\frac{1+\frac{J_{\mathrm{OVOCs}}[\mathrm{OVOCs}]}{R_{\mathrm{ALD}}[\mathrm{OH}]}}{1+\frac{R_{\mathrm{NO_2}}}{R_{\mathrm{ALD}}}+\frac{k_{\mathrm{OH+NO_2}}k_{\mathrm{PA+NO}}[\mathrm{NO}]}{k_{\mathrm{PA+NO_2}}R_{\mathrm{ALD}}}+\frac{J_{\mathrm{OVOCs}}[\mathrm{OVOCs}]}{R_{\mathrm{ALD}}[\mathrm{OH}]}} \quad \text{(S6)}$$

S6 Model sensitivity analysis

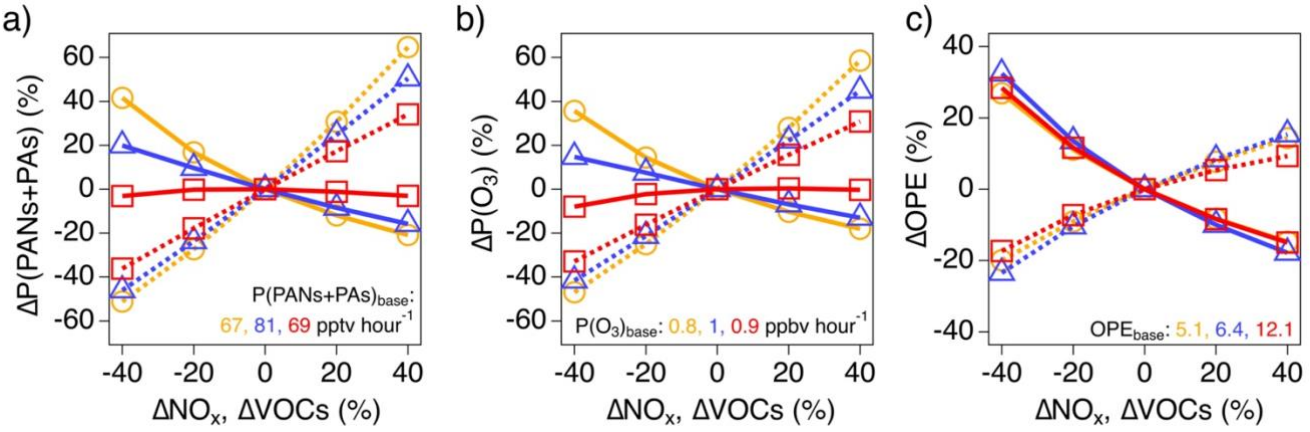

Figure S8. Model sensitivity of (a) P(PANs), (b) $P(O_3)$ and (c) OPE to ±40% changes in NO_x and VOCs constraints, along with the corresponding base-case values.

References

Apel, E. C., Hornbrook, R. S., Hills, A. J., Blake, N. J., Barth, M. C., Weinheimer, A., Cantrell, C., Rutledge, S. A., Basarab, B., Crawford, J., Diskin, G., Homeyer, C. R., Campos, T., Flocke, F., and Fried, A.: Upper tropospheric ozone production from lightning NO_x-impacted convection: Smoke ingestion case study from the DC3 campaign, J. Geophys. Res.-Atmos., 120, 2505–2523, https://doi.org/10.1002/2014JD022121, 2015.

Bahreini, R., Ervens, B., Middlebrook, A. M., Warneke, C., de Gouw, J. A., DeCarlo, P. F., Jimenez, J. L., Brock, C. A., Neuman, J. A., Ryerson, T. B., Stark, H., Atlas, E., Brioude, J., Fried, A., Holloway, J. S., Peischl, J., Richter, D., Walega, J., Weibring, P., Wollny, A. G., and Fehsenfeld, F. C.: Organic aerosol formation in urban and industrial plumes near Houston and Dallas, Texas, J. Geophys. Res.-Atmos., 114, D00F16, https://doi.org/10.1029/2008JD011493, 2009.

Bertman, S. B., Roberts, J. M., Parrish, D. D., Buhr, M. P., Goldan, P. D., Kuster, W. C., Fehsenfeld, F. C., Montzka, S. A., and Westberg, H.: Evolution of alkyl nitrates with air mass age, J. Geophys. Res.-Atmos., 100, 22805–22813, https://doi.org/10.1029/95JD02030, 1995.

Bourgeois, I., Peischl, J., Neuman, J. A., Brown, S. S., Allen, H. M., Campuzano-Jost, P., Coggon, M. M., DiGangi, J. P., Diskin, G. S., Gilman, J. B., Gkatzelis, G. I., Guo, H., Halliday, H. A., Hanisco, T. F., Holmes, C. D., Huey, L. G., Jimenez, J. L., Lamplugh, A. D., Lee, Y. R., Lindaas, J., Moore, R. H., Nault, B. A., Nowak, J. B., Pagonis, D., Rickly, P. S., Robinson, M. A., Rollins, A. W., Selimovic, V., St. Clair, J. M., Tanner, D., Vasquez, K. T., Veres, P. R., Warneke, C., Wennberg, P. O., Washenfelder, R. A., Wiggins, E. B., Womack, C. C., Xu, L., Zarzana, K. J., and Ryerson, T. B.: Comparison of airborne measurements of NO, NO_2, HONO, NO_y, and CO during FIREX-AQ, Atmos. Meas. Tech., 15, 4901–4930, https://doi.org/10.5194/amt-15-4901-2022, 2022.

Cazorla, M., Wolfe, G. M., Bailey, S. A., Swanson, A. K., Arkinson, H. L., and Hanisco, T. F.: A new airborne laser-induced fluorescence instrument for in situ detection of formaldehyde throughout the troposphere and lower stratosphere, Atmos. Meas. Tech., 8, 541–552, https://doi.org/10.5194/amt-8-541-2015, 2015.

Crounse, J. D., McKinney, K. A., Kwan, A. J., and Wennberg, P. O.: Measurement of gas-phase hydroperoxides by chemical ionization mass spectrometry, Anal. Chem., 78, 6726–6732, https://doi.org/10.1021/ac0604235, 2006.

de Gouw, J. A., Gilman, J. B., Kim, S.-W., Lerner, B. M., Isaacman-VanWertz, G., McDonald, B. C., Warneke, C., Kuster, W. C., Lefer, B. L., Griffith, S. M., Dusanter, S., Stevens, P. S., and Stutz, J.: Chemistry of Volatile Organic Compounds in the Los Angeles basin: Nighttime Removal of Alkenes and Determination of Emission Ratios, J. Geophys. Res.-Atmos., 122, 11843–11861, https://doi.org/10.1002/2017JD027459, 2017.

Diskin, G. S., Podolske, J. R., Sachse, G. W., and Slate, T. A.: Open-path airborne tunable diode laser hygrometer, Proc. SPIE, 4817, 196–204, https://doi.org/10.1117/12.453736, 2002.

Farmer, D. K., Perring, A. E., Wooldridge, P. J., Blake, D. R., Baker, A., Meinardi, S., Huey, L. G., Tanner, D., Vargas, O., and Cohen, R. C.: Impact of organic nitrates on urban ozone production, Atmos. Chem. Phys., 11, 4085–4094, https://doi.org/10.5194/acp-11-4085-2011, 2011.

Fisher, J. A., Atlas, E. L., Barletta, B., Meinardi, S., Blake, D. R., Thompson, C. R., Ryerson, T. B., Peischl, J., Tzompa-Sosa, Z. A., and Murray, L. T.: Methyl, ethyl, and propyl nitrates: global distribution and impacts on reactive nitrogen in remote marine environments, J. Geophys. Res.-Atmos., 123, 12429–12451, https://doi.org/10.1029/2018JD029046, 2018.

Guo, H., Campuzano-Jost, P., Nault, B. A., Day, D. A., Schroder, J. C., Kim, D., Dibb, J. E., Dollner, M., Weinzierl, B., and Jimenez, J. L.: The importance of size ranges in aerosol instrument intercomparisons: a case study for the Atmospheric Tomography Mission, Atmos. Meas. Tech., 14, 3631–3655, https://doi.org/10.5194/amt-14-3631-2021, 2021.

Hall, S. R., Ullmann, K., Prather, M. J., Flynn, C. M., Murray, L. T., Fiore, A. M., Correa, G., Strode, S. A., Steenrod, S. D., Lamarque, J.-F., Guth, J., Josse, B., Flemming, J., Huijnen, V., Abraham, N. L., and Archibald, A. T.: Cloud impacts on photochemistry: building a climatology of photolysis rates from the Atmospheric Tomography mission, Atmos. Chem. Phys., 18, 16809–16828, https://doi.org/10.5194/acp-18-16809-2018, 2018.

Hannun, R. A., Swanson, A. K., Bailey, S. A., Hanisco, T. F., Bui, T. P., Bourgeois, I., Peischl, J., and Ryerson, T. B.: A cavity-enhanced ultraviolet absorption instrument for high-precision, fast-time-response ozone measurements, Atmos. Meas. Tech., 13, 6877–6887, https://doi.org/10.5194/amt-13-6877-2020, 2020.

Hornbrook, R. S., Hills, A. J., Riemer, D., Abdelhamid, A., Flocke, F. M., Hall, S. R., Huey, L. G., Knapp, D. J., Liao, J., Mauldin III, R. L., Montzka, D. D., Orlando, J. J., Shepson, P. B., Sive, B., Staebler, R. M., Tanner, D. J., Thompson, C. R., Turnipseed, A., Ullmann, K., Weinheimer, A. J., and Apel, E. C.: Arctic springtime observations of volatile organic compounds during the OASIS-2009 campaign, J. Geophys. Res.Atmos., 121, 9789–9813, https://doi.org/10.1002/2015JD024360, 2016.

Ji, Y., Huey, L. G., Tanner, D. J., Lee, Y. R., Veres, P. R., Neuman, J. A., Wang, Y., and Wang, X.: A vacuum ultraviolet ion source (VUV-IS) for iodide–chemical ionization mass spectrometry: a substitute for radioactive ion sources, Atmos. Meas. Tech., 13, 3683–3696, https://doi.org/10.5194/amt-13-3683-2020, 2020.

Lee, Y. R., Ji, Y., Tanner, D. J., and Huey, L. G.: A low-activity ion source for measurement of atmospheric gases by chemical ionization mass spectrometry, Atmos. Meas. Tech., 13, 2473–2480, https://doi.org/10.5194/amt-13-2473-2020, 2020.

McKeen, S. A. and Liu, S. C.: Hydrocarbon ratios and photochemical history of air masses, Geophys. Res. Lett., 20, 2363–2366, https://doi.org/10.1029/93GL02527, 1993.

Moore, R. H., Wiggins, E. B., Ahern, A. T., Zimmerman, S., Montgomery, L., Campuzano Jost, P., Robinson, C. E., Ziemba, L. D., Winstead, E. L., Anderson, B. E., Brock, C. A., Brown, M. D., Chen, G., Crosbie, E. C., Guo, H., Jimenez, J. L., Jordan, C. E., Lyu, M., Nault, B. A., Rothfuss, N. E., Sanchez, K. J., Schueneman, M., Shingler, T. J., Shook, M. A., Thornhill, K. L., Wagner, N. L., and Wang, J.: Sizing response of the Ultra-High Sensitivity Aerosol Spectrometer (UHSAS) and Laser Aerosol Spectrometer (LAS) to changes in submicron aerosol composition and refractive index, Atmos. Meas. Tech., 14, 4517–4542, https://doi.org/10.5194/amt-14-4517-2021, 2021.

Nault, B. A., Campuzano-Jost, P., Day, D. A., Schroder, J. C., Anderson, B., Beyersdorf, A. J., Blake, D. R., Brune, W. H., Choi, Y., Corr, C. A., de Gouw, J. A., Dibb, J., DiGangi, J. P., Diskin, G. S., Fried, A., Huey, L. G., Kim, M. J., Knote, C. J., Lamb, K. D., Lee, T., Park, T., Pusede, S. E., Scheuer, E., Thornhill, K. L., Woo, J.-H., and Jimenez, J. L.: Secondary organic aerosol production from local emissions dominates the organic aerosol budget over Seoul, South Korea, during KORUS-AQ, Atmos. Chem. Phys., 18, 17769–17800, https://doi.org/10.5194/acp-18-17769-2018, 2018.

Parrish, D. D., Stohl, A., Forster, C., Atlas, E. L., Blake, D. R., Goldan, P. D., Kuster, W. C., and de Gouw, J. A.: Effects of mixing on evolution of hydrocarbon ratios in the troposphere, J. Geophys. Res.-Atmos., 112, D10S34, https://doi.org/10.1029/2006JD007583, 2007.

Perring, A. E., Pusede, S. E., and Cohen, R. C.: An observational perspective on the atmospheric impacts of alkyl and multifunctional nitrates on ozone and secondary organic aerosol, Chem. Rev., 113, 5848–5870, https://doi.org/10.1021/cr300520x, 2013.

Reinecke, T., Leiminger, M., Jordan, A., Wisthaler, A., and Müller, M.: Ultrahigh sensitivity PTR-MS instrument with a well-defined ion chemistry, Anal. Chem., 95, 11879–11884, https://doi.org/10.1021/acs.analchem.3c02669, 2023.

Rosen, R. S., Wood, E. C., Wooldridge, P. J., Thornton, J. A., Day, D. A., Kuster, W., Williams, E. J., Jobson, B. T., and Cohen, R. C.: Observations of total alkyl nitrates during Texas Air Quality Study 2000: Implications for O_3 and alkyl nitrate photochemistry, J. Geophys. Res.-Atmos., 109, D07303, https://doi.org/10.1029/2003JD004227, 2004.

Sachse, G. W., Collins Jr., J. E., Hill, G. F., Wade, L. O., Burney, L. G., and Ritter, J. A.: Airborne tunable diode laser sensor for high-precision concentration and flux measurements of carbon monoxide and methane, Proc. SPIE, 1433, 157–166, https://doi.org/10.1117/12.46162, 1991.

Sachse, G. W., Hill, G. F., Wade, L. O., and Perry, M. G.: Fast-response, high-precision carbon monoxide sensor using a tunable diode laser absorption technique, J. Geophys. Res.-Atmos., 92, 2071–2081, https://doi.org/10.1029/JD092iD02p02071, 1987.

Simpson, I. J., Blake, D. R., Blake, N. J., Meinardi, S., Barletta, B., Hughes, S. C., Fleming, L. T., Crawford, J. H., Diskin, G. S., Emmons, L. K., Fried, A., Guo, H., Peterson, D. A., Wisthaler, A., Woo, J.-H., Barré, J., Gaubert, B., Kim, J., Kim, M. J., Kim, Y., Knote, C., Mikoviny, T., Pusede, S. E., Schroeder, J. R., Wang, Y., Wennberg, P. O., and Zeng, L.: Characterization, sources and reactivity of volatile organic compounds (VOCs) in Seoul and surrounding regions during KORUS-AQ, Elem. Sci. Anth., 8, 37, https://doi.org/10.1525/elementa.434, 2020.

Slusher, D. L., Huey, L. G., Tanner, D. J., Flocke, F. M., and Roberts, J. M.: A thermal dissociation–chemical ionization mass spectrometry (TD-CIMS) technique for the simultaneous measurement of peroxyacyl nitrates and dinitrogen pentoxide, J. Geophys. Res.-Atmos., 109, D19315, https://doi.org/10.1029/2004JD004670, 2004.

St. Clair, J. M., Swanson, A. K., Bailey, S. A., and Hanisco, T. F.: CAFE: a new, improved nonresonant laser-induced fluorescence instrument for airborne in situ measurement of formaldehyde, Atmos. Meas. Tech., 12, 4581–4590, https://doi.org/10.5194/amt-12-4581-2019, 2019.

Teng, A. P., Crounse, J. D., Lee, L., St. Clair, J. M., Cohen, R. C., and Wennberg, P. O.: Hydroxy nitrate production in the OH-initiated oxidation of alkenes, Atmos. Chem. Phys., 15, 4297–4316, https://doi.org/10.5194/acp-15-4297-2015, 2015.

Weinheimer, A. J., Walega, J. G., Ridley, B. A., Gary, B. L., Blake, D. R., Blake, N. J., Rowland, F. S., Sachse, G. W., Anderson, B. E., and Collins, J. E.: Meridional distributions of NO_x, NO_y, and other species in the lower stratosphere and upper troposphere during AASE II, Geophys. Res. Lett., 21, 2583–2586, https://doi.org/10.1029/94GL01897, 1994.